ARTICLE

Surface-Directed Dewetting of a Block Copolymer for Fabricating Highly Uniform Nanostructured Microdroplets and Concentric Nanorings

Richard A. Farrell,[†,‡,§] Nikolaos Kehagias,[⊥] Matthew T. Shaw,[‡,¶] Vincent Reboud,[⊥] Marc Zelsmann,[#] Justin D. Holmes,[†,‡,§] Clivia M. Sotomayor Torres,[⊥,||] and Michael A. Morris[†,‡,§,*]

[†]Department of Chemistry, University College Cork, Cork, Ireland, [‡]Centre for Research on Adaptive Nanostructures and Nanodevices (CRANN), Trinity College Dublin, Dublin 2, Ireland, [§]Tyndall National Institute, Lee Maltings, Prospect Row, Cork, Ireland, [⊥]Catalan Institute of Nanotechnology, Campus de Bellaterra, Edifici CM7, ES 08193 Bellaterra, Barcelona, Spain, [||]Catalan Institute of Research and Advanced Studies (ICREA), 08010 Barcelona, Spain, [¶]Intel Ireland Limited, Collinstown Industrial Estate, Leixlip, Co. Kildare, Ireland, and [#]Laboratoire des Technologies de la Microélectronique (CNRS), 38054 Grenoble, France

ABSTRACT Through a combination of nanoimprint lithography and block copolymer self-assembly, a highly regular dewetting process of a symmetric diblock copolymer occurs whereby the hierarchal formation of microdroplets and concentric nanorings emerges. The process is driven by the unique chemical properties and geometrical layout of the underlying patterned silsesquioxane micrometer-sized templates. Given the presence of nonpreferential substrate−polymer interactions, directed dewetting was utilized to produce uniform arrays of microsized droplets of microphase separated polystyrene-*block*-poly(methyl methylacrylate) (PS-*b*-PMMA), following thermal annealing at 180 °C. Microdroplets with diameters greater than 400 nm exhibited a hexagonal close-packed arrangement of nanodots on the surface with polydomain ordering. At the droplet periphery, the polydomain ordering was severely disrupted because of a higher in-plane radius of curvature. By reducing the droplet size, the in-plane radius of curvature of the microdroplet becomes significant and the PMMA cylinders adopt parallel structures in this confined geometry. Continuous scaling of the droplet results in the generation of isolated, freestanding, self-aligned, and self-supported oblique nanorings (long axis ∼250−350 nm), which form as interstitial droplets between the larger microdroplets. Optical and magnetic-based nanostructures may benefit from such hierarchal organization and self-supporting/aligned nanoring templates by combining more than one lithography technique with different resolution capabilities.

KEYWORDS: block copolymers · directed dewetting · nanoimprint lithography · silsesquioxane · graphoepitaxy · polystyrene-*block*-poly(methyl methylacrylate) · nanoring · microdroplet

Block copolymers (BCPs) comprise two or more constituent polymers tethered together by a covalent bond. Consequently, these polymers when heated above their glass transition temperature (T_g), but below their order−disorder transition temperature (ODT), microphase separate and form periodic nanostructures. Depending on their molar fraction (ratio of block A to other constituent blocks), molecular weight, and segmental interaction parameter (Flory−Huggins parameter), various morphologies such as hexagonal, lamellae, or closed-packed spherical, with critical dimensions ranging from 5 to 50 nm, can be formed.[1] When confined as a thin film, the orientational and translational ordering of block copolymers can be perturbed by the close proximity of substrate and air interfaces resulting in preferred orientations.[2,3] Furthermore, although the polymer films may have a defined orientation, their translational ordering is limited due to the presence of competing polydomains.[4] Methods for correcting this loss of translational ordering in PS-*b*-PMMA thin films, for example, include chemical epitaxy,[5] graphoepitaxy using photoresist materials,[6,7] and nanoimprint lithography.[8]

Dewetting instabilities in polymeric thin films are recognized to occur due to incompatible interfacial energies between the film and the substrate.[9,10] To date, two different mechanisms for dewetting of polymer thin films, nucleation/growth, and spinodal decomposition have been identified.[11,12] Factors such as film thickness, polymer−surface interaction, molecular weight, viscosity, and substrate surface tension all play a crucial role in polymer dewetting processes.[13] Recently, researchers have attempted to control this dewetting phenomenon for polymer films by using microcontact printing (μCP)[14,15] and nanoimprint lithography[16] to create microscale patterns.

Block copolymer thin films are also prone to dewetting instabilities. Understanding factors such as the interplay between the quantized film thickness and the intrinsic polymer length scale, the tendency for one of the

*Address correspondence to m.morris@ucc.ie.

Received for review October 11, 2010 and accepted December 30, 2010.

Published online January 12, 2011
10.1021/nn102720m

© 2011 American Chemical Society

blocks to preferentially wet an interface (*i.e.*, asymmetric and symmetric wetting) and the possibility of autophobic dewetting are essential for controlling dewetting of block polymer systems.[13,17−19] Early studies focused on the dewetting of block copolymers to create 10−30 μm sized PS-*b*-PMMA annular structures, which showed preferential radial alignment of the PMMA cylinders at the rims of the annular structures.[20] Recently, Croll and co-workers have utilized dewetting to create PS-*b*-PMMA microdroplets with terraced hyperbolic structures by thermal annealing techniques.[21] In the isotropic state, the droplet assumed a spherical shape but, upon thermal annealing, transitioned to the anisotropic state; hence the droplet became terraced and adopted a hyperbolic profile as a result of microphase separation. The authors suggested that two competing actions led to the hyperbolic structure: edge tension and edge repulsion.[21,22] Alternatively, Hong *et al.* have employed controlled evaporation-induced self-assembly of block copolymers by placing the drying droplet under a sphere-on-silicon geometry to fabricate hierarchal serpentine microstructures. The difference in the interfacial energies of the polymer and substrate results in fingering instabilities within the film and the formation of hierarchal serpentine structures.[23] Subsequently, further exposure to acetone vapors facilitated microphase separation of the PS-*b*-PMMA on the nanoscale with cylinders oriented perpendicular to the substrate. Furthermore, dewetting instabilities can be directed to create mesoscale dendritic hierarchal poly(styrene-*block*-ferrocenyldimethylsilane) structures by employing a combination of solvent and thermal annealing. Again, this type of multiscale lithography approach has potential to pattern on different length scales for microelectronic and photonic applications.[24]

PS-*b*-PEO films are recognized to dewet the substrate during solvent annealing because of small changes in the interfacial chemistry between the solvent-swollen film and the substrate.[25] Using dewetting to their advantage, Kim *et al.*[26] formed hierarchal structures by intentionally dewetting a PS-*b*-PEO film on prepatterned surface-adsorbed monolayer (SAM) surfaces manufactured by microcontact printing techniques. Microphase separation and dewetting simultaneously occurred when the PS-*b*-PEO films were swelled in a benzene atmosphere. By directing the dewetting process, the authors were able to fabricate convex lens-shaped caps over 1 mm^2 regions with extremely high regularity. Recently, researchers have developed a method for spontaneously aligning symmetric lamellae PS-*b*-PMMA films by depositing the BCP onto micropatterned strips and inducing thermal dewetting over extremely large dimensions to create films with micrometer-sized undulations.[27] Consequently, the lamellae patterns were aligned in the direction of the thickness gradient by a mechanism known as "geometrical anchoring", whereby tilting of the domains led to a minimization of the overall elastic energy of the PS-*b*-PMMA film when confined under nonflat geometry conditions.[28] The authors focused mainly on microstrip patterns but also showed preliminary results for individual 100 μm sized droplets.

Previous work on aligning block copolymer nanopatterns (by graphoepitaxy) within electron beam patterned hydrogen silsesquioxane (HSQ)-type templates have demonstrated that line and concentric hexagonal arrays of PS-*b*-PMMA lamellae patterns can be assembled with precision.[29] The combination of using a neutral brush layer at the base and a hydrogen silsesquioxane (HSQ) sidewall allowed the creation of hexagonal arrays of parallel cylinders and concentric rings of two PMMA cylinders with low defect content. Extremely thin layers (~2 nm) of hydrogen silsesquioxane have also been written by electron beam methods to create chemical patterns (14 nm half-pitch) to align and register PS-*b*-PMMA patterns.[30] More importantly, sparse chemical patterns of these HSQ lines with spacers that were double, triple, and quadruple that of the natural periodicity of the BCP were shown to direct the self-assembly of the nanopatterns, thus representing a 4-fold resolution enhancement when combined with top-down lithographic techniques.[30] Furthermore, concentric rings were also generated using this approach; 140 concentric PMMA rings could readily be fabricated without any discernible loss in translational ordering. Although direct write exposure of HSQ patterns have yielded well-aligned linear and concentric ring structures of PS-*b*-PMMA structures, electron beam patterning of HSQ is restricted by its low sensitivity and stability.[31,32]

Block copolymers, because of their flexibility, can be fashioned into nanoring structures by graphoepitaxy[33] and chemical patterning.[30,34] Ferromagnetic nanostructures which have a ring structure are of interest because they have stable magnetic states (onion and vortex) at remanence and, as a result, may find uses in magnetic RAM applications.[35] Nanoring structures have recently been reported for PS-*b*-PMMA,[34] PS-*b*-P4VP (polystyrene-*block*-(4-vinylpyridine)),[36,37] and PS-*b*-PFS-*b*-P2VP (polystyrene-*block*-(ferrocenyldimethylsilane)-*block*-(2-vinylpyridine))[33] block copolymers by either tuning their hydrophobicity or by implementing chemical/physical prepatterning techniques.

Herein, patterned silsesquioxane (SSQ) films with varying dimensions of via-hole and linear arrays have been fabricated using a reverse ultraviolet nanoimprint lithography (RUV-NIL[38]) technique to investigate the self-assembling properties and polymer flow/dewetting phenomena of asymmetric polystyrene-*block*-poly(methyl methylacrylate) block copolymer films. Directed dewetting was utilized to produce uniform arrays of micro/nanosized droplets whereby the PS-*b*-PMMA polymer simultaneously undergoes microphase separation, dewets the methylated surface, and flows into via-holes to minimize its surface energy during thermal annealing. The droplet size was readily controlled by adjusting the pitch and via-hole dimensions,

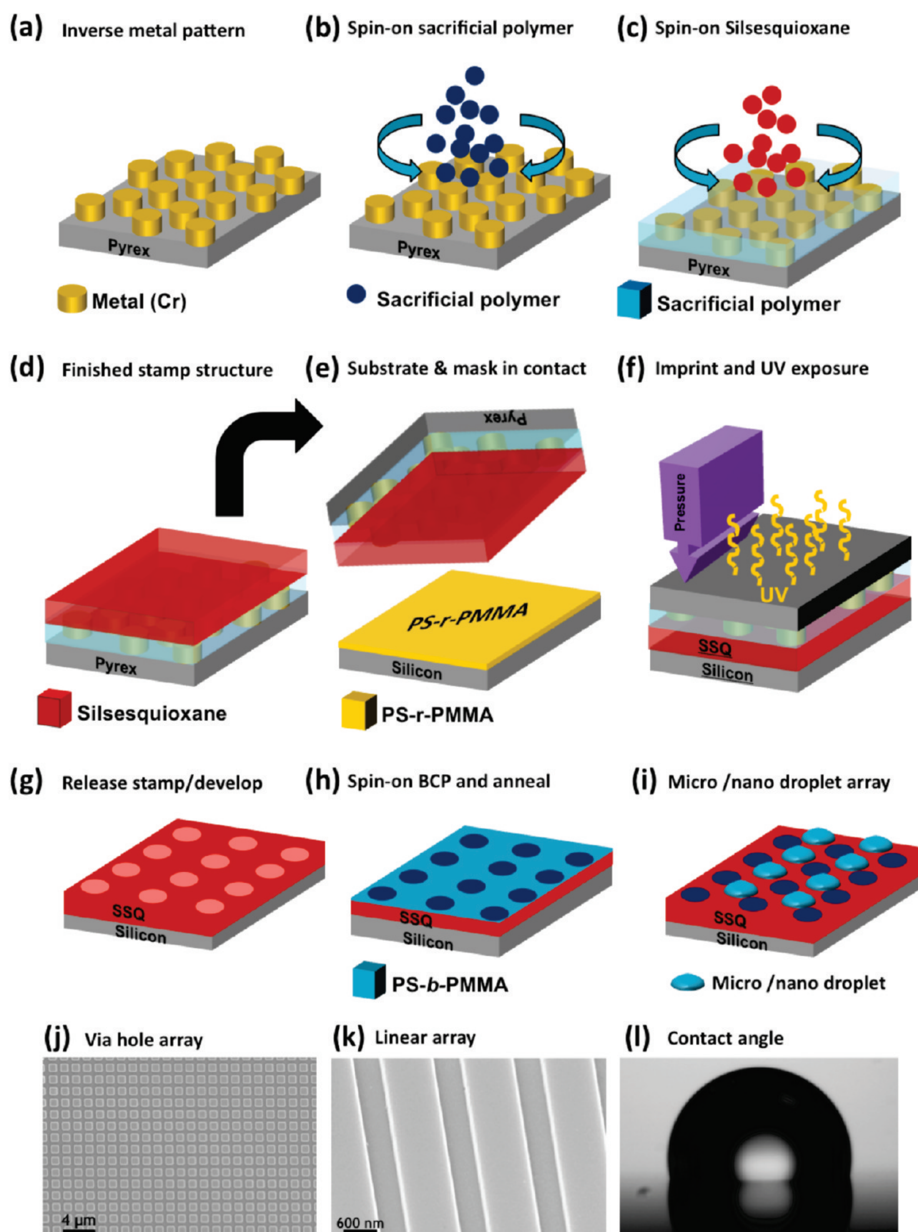

Figure 1. (a−i) Schematic 3D process flow diagram for creating patterned SSQ films by RUV-NIL technique. Top-down SEM images of NIL prepared SSQ (j) via-hole arrays and (k) line arrays prior to block copolymer deposition and dewetting and (l) optical image of contact angle ~100° measured on a planar SSQ surface post-UV curing. The scale bars in images (j) and (k) are 4 μm and 600 nm, respectively.

which circumvented droplets from merging. In addition, it was possible to fabricate isolated concentric nanoring structures with two PMMA cylinders (250−350 nm), which formed between the larger microdroplets without the need for extreme confinement and avoiding expensive lithographic techniques.

RESULTS AND DISCUSSION

Imprinting and Thin Film Wetting. Nanoimprinting of a UV-curable silsesquioxane thin film presents the opportunity to access its unique chemical (methylated surface) and photopatternable properties, whereas conventional patterning techniques which employ post-plasma processing (surface oxidation) do not. Line and via-hole arrays with spacer and critical dimensions ranging from 400 to 4000 nm (mesa and trench were approximately equal in lateral dimensions) were created in SSQ inorganic polymer films using an RUV-NIL process. Briefly, as outlined in Figure 1a−i, the inverse metallic patterns of the desired layout and dimensions were first created on a transparent quartz substrate. A sacrificial polymer layer was deposited prior to the SSQ deposition to ensure effective release after UV exposure. The Pyrex/metallic template/sacrificial polymer/silsesquioxane stack was brought into contact with the silicon substrate and imprinted for 60 s at 6 bar followed by a 5 s UV exposure to ensure cross-linking of the silsesquioxane. Finally, the stack

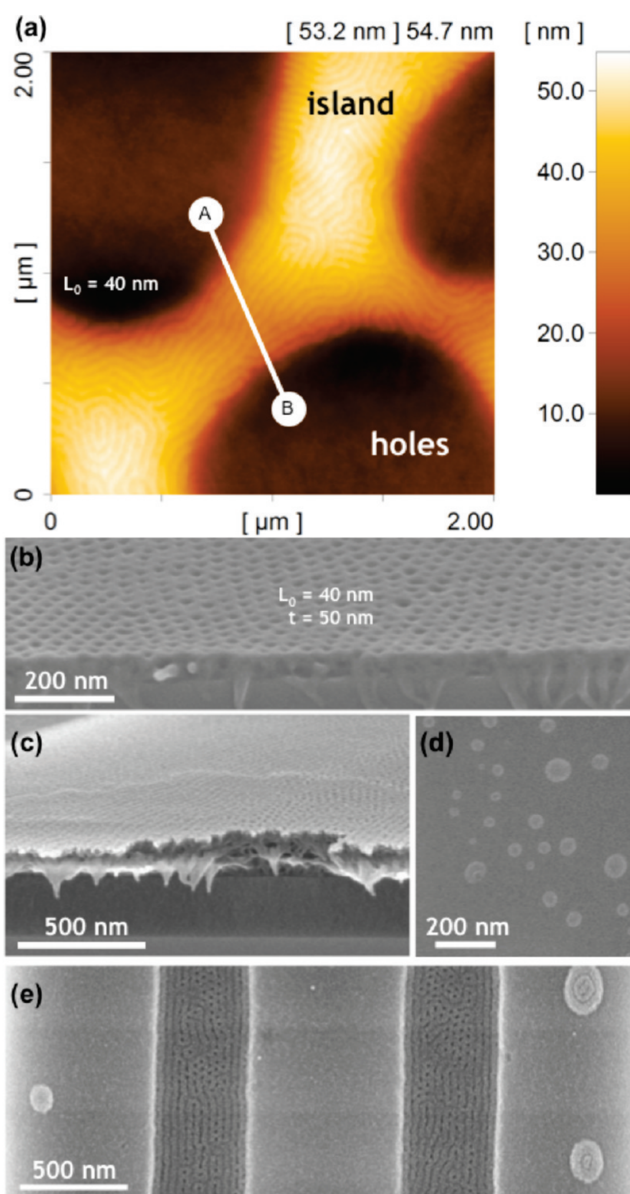

Figure 2. PMMA cylinder orientation: (a) 2D AFM tapping mode height image (step height from A to B of 33 nm) of the island and hole formation for a 0.7% wt PS-*b*-PMMA (46−21 kg/mol) on native silicon dioxide, where cylinders are arranged parallel to substrate; (b) 70° cross-sectional SEM tilt image of a PS-*b*-PMMA (46−21 kg/mol) deposited from a 1.5% wt solution on ∼5 nm PS-*r*-PMMA, where cylinders are arranged perpendicular to the substrate; (c) 70° tilt SEM image of large droplets of PS-*b*-PMMA after dewetting on an SSQ surface; (d) top-down SEM image of small droplets PS-*b*-PMMA after dewetting on an SSQ surface; and (e) partial alignment of PS-*b*-PMMA nanopatterns in patterned arrays of SSQ with nanoring formation on the mesas.

and the silicon substrate were released, and the SSQ developed in tetramethylammoniumhydroxide (TMAOH), resulting in the formation of the topographic SSQ patterns. Top-down SEM images of the patterned SSQ structures on brush-coated silicon substrates are shown in Figure 1j,k. The fidelity of the pattern transfer from the RUV-NIL process was not of strict importance for the current study as only the via-holes were required to act as guides. A residual layer of approximately 100 nm remained from the imprinting process, while the resultant line and via-hole patterns had significant rounding (Supporting Information Figure S1b,e). Figure 1l is an image of a water droplet residing on a planar SSQ surface. Contact angles for the planar SSQ films ranged from 96 to 107°, highlighting the extent of surface methyl ($-CH_3$) groups present. The hydrophobic surface was essential for creating periodic micro/nanoscale droplets.

Figure 2 highlights the importance of the interface between the substrate and block copolymer as this interaction ultimately influences the cylinder orientation in the asymmetric PS-*b*-PMMA and, more importantly, limits the polymers' ability to form a continuous and nanostructured film. Analysis of the asymmetric PS-*b*-PMMA block copolymer nanopatterns on silicon (native silicon dioxide) surfaces revealed the well-observed

phenomenon of island and hole formation (Figure 2a).[39] Generally, the PMMA (surface tension, γ_{PMMA} = 41.1 mN m^{-1}) has a preference for the polymer/substrate interface as it has a lower surface energy copolymer component, while the PS (surface tension, γ_{PS} = 40.7 mN m^{-1}) component favors the polymer/air interface.[40,41] However, for ultrathin film, both PS and PMMA domains can coexist at the polymer/air surface, as the surface energies are extremely close.[42] Figure 2a is a 2 × 2 μm AFM tapping mode image for an asymmetric PS-*b*-PMMA block copolymer deposited from a 0.7% weight solution in toluene on a native silicon dioxide surface. As a result of subtle surface tension variation between the two blocks, a PMMA wetting layer forms at the silicon interface with PMMA cylinders coexisting with the PS matrix at the polymer/air interface. FFT measurements reveal that the periodicity of the parallel PMMA cylinders (natural equilibrium distance, L_0) was ~40 nm, which agrees well with previous literature findings for asymmetric PS-*b*-PMMA with a M_w of 67 kg mol^{-1}.[43,44] Polymer islands form to minimize their free energy so as to be commensurate with the natural periodicity of the block copolymer. Under asymmetric wetting conditions, the thickness of block copolymer films becomes quantized as the film prefers to be commensurate with these quantized thickness values. Asymmetric wetting conditions dictate that a thickness of $(n + 0.5)L_0$ times the natural equilibrium length must be satisfied. For a 0.7% weight concentration, polymer islands form where the thickness satisfies this condition and the PMMA cylinders form fingerprint patterns within these islands. As the film is extremely thin, any polymer film in the hole sections is too thin (*i.e.*, < $1L_0$, and therefore, no nanopatterns are formed within these regions.[45] By grafting a random copolymer (neutral with respect to PS and PMMA) to the native silicon oxide, the PMMA affinity for the native silicon oxide surface can be decoupled and allow the microdomains to orient normal to the substrate (Figure 2b).[46−48] Consequently, a uniform film of PMMA cylinders in a PS matrix (film thickness ~50 nm) can be assembled on a neutral brush layer after annealing at 180 °C under vacuum for 24 h from a 1.5% weight solution. The natural cylinder-to-cylinder in-plane repeat distance was determined to be 40 nm (σ, 3.5 nm) with a cylinder diameter of approximately 20 nm from SEM and AFM (FFT calculations) data. Similar L_0 values were also measured for other studies involving asymmetric PS-*b*-PMMA with a M_w of 67 kg mol^{-1}.[44,49−51] For all SEM micrographs taken, the PS-*b*-PMMA microdroplets were exposed to an oxygen/trifluoromethane (O_2/CHF_3) reactive ion-etch to partially remove PMMA for imaging purposes.

PS-*b*-PMMA films on non-imprinted SSQ surfaces were found to behave quite differently to the native oxide and neutral brush surfaces. Surface dewetting is to be expected as surface tension values for SSQ (>20 mN m^{-1})[52] are quite different than that of the PS and PMMA. Under similar thermal and preparatory conditions, neither PS nor PMMA segments favorably wetted the highly methylated SSQ surface and, consequently, gave rise to non-uniform and random arrays of droplets with sizes ranging from the sub-100 nm to well beyond the micrometer scale (Figure 2c,d). Figure 2c displays a tilt SEM image of a large droplet (>2 μm) that has undergone microphase separation but has also dewetted from the surface and formed large uncontrollably globular-like structures. In other regions (Figure 2d), the polymer can be seen to form smaller droplets with sizes ranging from 20 to 100 nm, highlighting the variation in the dewetting process on the SSQ surface.

Microdroplet Formation on Patterned Silsesquioxane Surfaces. Our motivation for the following study originated from frequently observing the formation of microdroplets on planar SSQ substrates (Figure 2d) and, in some cases, self-supporting nanorings from our investigations relating to aligning PS-*b*-PMMA nanopatterns by graphoepitaxy (Figure 2e and Supporting Information section S1) techniques on these SSQ patterns. Overall, the inaccessibility to the brush layer, owing to the presence of the NIL residual layer and rounding of the SSQ profile, limited these investigations. Consequently, residual polymer located on mesas during graphoepitaxy studies has prompted recent work on reducing the mesa itself to very small dimensions[53] by replacing the mesa with sparse pillars with feature sizes similar to that of the BCP[54] or by employing a disposable resist followed by a chemical patterning approach.[7]

As highlighted in Figure 3, chemical interactions between the substrate and block copolymer are important for controlling the wetting and film thickness (orientation) of the film. With this in mind and the knowledge of droplet formation during graphoepitaxy experiments, it was possible to localize these structures in desired locations across arrays of via-holes. By depositing 1 wt % solutions of PS-*b*-PMMA (46−21 kg mol^{-1}) on arrays of via-holes and annealing at 180 °C for 24 h, a highly regular dewetting process was found to take place. Optical microscopy analysis (Figure 3a,b) confirms that the dewetting process was extremely effective and extended well beyond the 50 μm scale. On closer inspection of the arrays, we found that each microdroplet (orange) was surrounded by four via-holes (orange with black ring). Microphase separation was observed for all droplet structures on the interstitial mesa positions and within neighboring via-hole structures. For our investigations, rather than adjusting the weight percentage of the BCP, the via-hole spacer and occasionally the via-hole dimension were varied to control the dewetting process. Figure 3c displays a SEM image of the microdroplet formation on the SSQ pattern. In this instance, the 675 nm spherical microdroplets (Figure 3d) were precisely positioned within the center of each 1100 nm diagonal mesa with a nearest neighbor distance of approximately 700 nm. During thermal annealing,

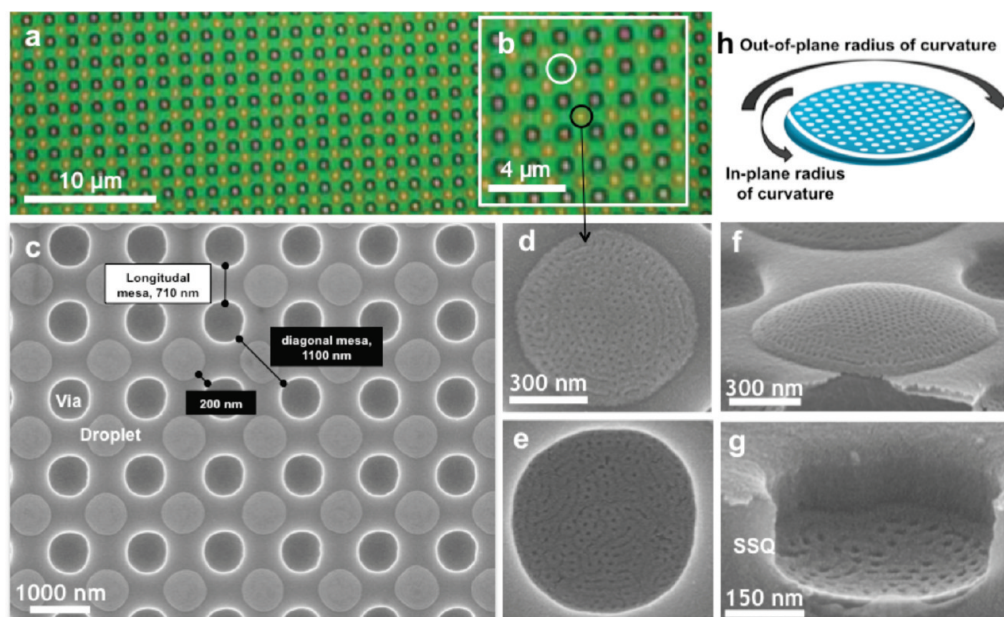

Figure 3. (a,b) Optical microscopy and (c) SEM images of a regular array of ∼675 nm microdroplets formed on top of the diagonal mesas between the 600 nm via-holes as a result of dewetting processes for a 1% wt PS-PMMA (46−21 kg/mol) solution; (d,e) SEM images of microphase separation within the microdroplet on the mesa and within the via-hole (reservoir) taken from image (d); (f,g) 70° tilt SEM images of microphase separation within a microdroplet on SSQ mesas and via-holes; (h) 3D graphic of a droplet defining the in-plane and out-of-plane radii of curvature.

the as-deposited film ruptures due to nonfavorable wetting between both PS (surface tension, γ_{PS} = 40.7 mN m^{-1}) and PMMA (surface tension, γ_{PMMA} = 41.1 mN m^{-1}) and the SSQ (surface tension, γ_{SSQ} < 20 mN m^{-1}) substrate. This rupturing acts to minimize surface energy by producing microdroplets. The hydrophobic SSQ template or, more importantly, the via-hole structures act as guides to direct the formation of this dewetting process while simultaneously sequestering polymer in the holes as a result of capillary forces (Figure 3e). As the surface was extremely methylated (as observed from contact angles of approximately 100°), the majority PS component preferentially wets the fully cross-linked SSQ surface, resulting in a symmetric wetting regime. Recently, similar studies by Suh *et al.* confirmed that, when silsesquioxane surfaces are fully cured at 400 °C, the PS tends to wet the SSQ surface rather than the PMMA.[55] Figure 3f,g shows tilt SEM images that provide three-dimensional topographical information on both the droplet and surplus polymer in a via-hole. The microdroplets formed spherical cap-like structures, while the polymer within the via-hole formed an inverse cap to compensate for the rounded profile of the hole from the RUV-NIL process. Interestingly, polymer within the actual via-hole (Figure 3g) was microphase separated, although the polymer structure within the via-hole is significantly perturbed with cylinders oriented in both parallel and perpendicular orientations. The mixed morphology can be attributed to changes in droplet thickness caused by the rounded profile of the via-hole. Tuning the dimensions of the physical prepattern prior to polymer deposition can easily create microdroplet sizes ranging from *ca.* 400 to 2500 nm.

Droplet Topographic and Internal Nanostructure. PS-*b*-PMMA microphase separation has been well-studied for planar continuous films, and it has been established that film thickness and surface boundary conditions dictate the outcome of the final orientation.[45,56] Such behavior is also observed within the microdroplets due to the changing thickness of the droplet and the hydrophobic SSQ surface. Consequently, three regions of interest exist which require investigation: the droplet topography (excluding the 100 nm region at the edge), the droplet periphery, and the internal droplet structure. Before analysis of the orientation and morphology of the droplets is presented, it is important first to investigate the droplet thickness. Focused ion beam (FIB) cross sectioning was employed to ascertain thickness values of the droplet as a function of microdroplet diameter. Figure 4a (and Supporting Information Figure S2) displays a 54° tilt SEM image post-FIB cross sectioning of a 1000 nm droplet residing above the 400 nm SSQ film. To ensure preservation of the microdroplet during the physical etch process, electron and ion beam platinum layers were deposited prior to etching. Such is the polish created by this technique that any possibility of observing the internal nanoscale structure of the droplet is prohibited as the etch essentially creates a fine polish at the interface. The microdroplets adopt a convex, spherical cap shape which is prevalent across all microdroplet diameters. The droplet thickness at the center scales as a function of droplet diameter, where the droplet height was approximately 10 to 15% of

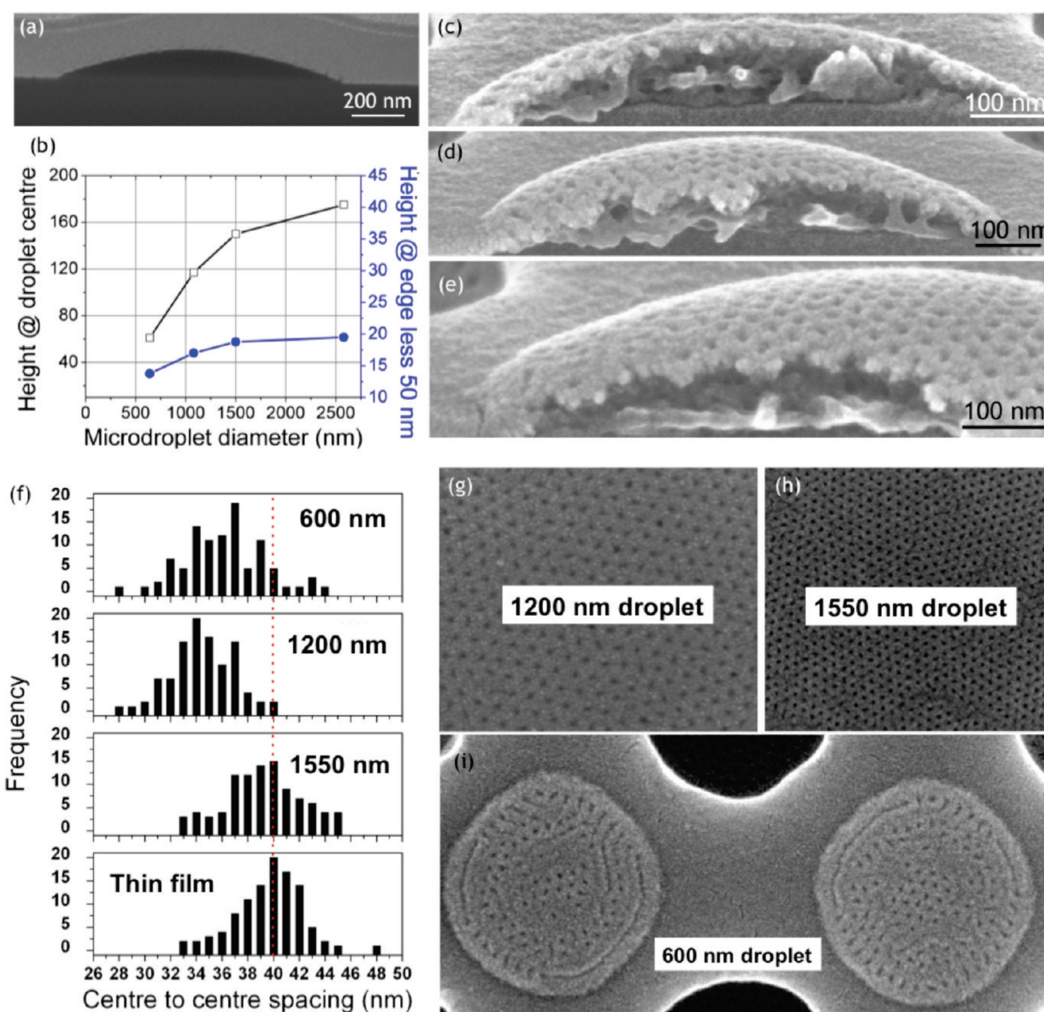

Figure 4. Droplet nanostructure and orientation: (a) 54° tilt SEM images post-FIB cross sectioning of a 1500 nm microdroplet. (b) Height of droplet at the center as a function of changing microdroplet diameter. Height measurements are taken at the droplet center and 50 nm in from the droplet edge to represent edge thickness. (c−e) The 70° tilt SEM images for 800 nm microdroplets sectioned by scribing to provide insight into the subsurface orientation and morphology. (f) Center-to-center spacing distributions for a thin film, 1550, 1200, and 600 nm microdroplet. (g−i) Regions that were sampled from the droplets. In the case of the 600 nm microdroplet, eight droplets were analyzed to provide more statistical information.

the droplet diameter, as shown in Figure 4b. Closer inspection of the thickness near the droplet edge (*i.e.*, 50 nm from edge) reveals that the thickness is well below an L_0 value of 40 nm and is close to 13 nm for a 600 nm microdroplet. The droplet thickness at the edge, even for the largest droplet, is approximately 40 nm or less (Figure 4b), which is close to the natural periodicity of the block copolymer.

Due to the fact that the microdroplet shape is convex (packing frustration of the polymer chains) and large droplets have thickness values close to 200 nm at the center,[2] it cannot be assumed that the surface structure extends into the bulk of the sample and that a hexagonal closed-packed arrangement of half cylinders or closed-packed spheres[45] may also exist at the surface. To establish the internal structure of the droplet, cross-sectional SEM techniques were employed to assist in determining the orientation and morphology within the droplets. In Figure 4c−e, the substructure was investigated by simple scribing techniques. Although the method provides more detail of the internal structure, it is limited by the fact that such a technique creates shear and tensile forces during breaking of the underlying SSQ film (and silicon substrate) and causes significant deformation (uncontrolled tearing) of the microdroplet. Furthermore, whereas topographic imaging of the droplets was achieved by introducing a partial etch of surface PMMA domains, only electron beam damage of PMMA during cross-sectional viewing can be used to provide contrast for viewing the substructure.[57] In some regions, spherical features close to 20 nm were observed, but since no large polydomain (*i.e.*, repetition of features/periodicity) behavior was evident, we cannot conclude that cylinders with a preferred morphology and vertical orientation exist within the bulk of the droplet or, more importantly, if a phase transition from hexagonal to spherical has transpired. Kim *et al.*[26] highlighted that the structure of a microdroplet consisting of asymmetric PS-*b*-PEO,

which predominantly forms a hexagonal closed-packed arrangement of cylinders in a continuous and uniform film, can undergo a domain phase transition to a spherical structure. The authors suggested that either significant swelling of the PS domain by benzene or the presence of a packing frustration, owing to the radius of curvature of the droplet, led to the phase transition. As our microphase separation technique is realized by thermal annealing under vacuum conditions, domain swelling is an unlikely event within the thermally dewetted PS-*b*-PMMA microdroplets.

The topographic structure consists of 20 nm holes arranged in a hexagonal closed-packed (hcp) configuration. To investigate topographic ordering, the natural periodicities of the various droplet sizes (Figure 4g−i) were measured. The defect density tends to increase drastically at the droplet edge because the radius of curvature becomes greater and the packing frustration of the polymer chains becomes more important, as confirmed by analyzing center-to-center spacings for various droplet diameters (Figure 4f). For simplicity, the center-to-center spacing measurements were performed at the center regions of the droplets (Supporting Information Figure S3), as extracting the center-to-center spacings was not possible at the edge due to the cylinder reorientation and the high defectivity. The average periodicity (L_0) of the PS-*b*-PMMA (67 kg mol^{-1}) thin film is approximately 40 nm, and depending on droplet size, the value decreases to 34 nm as droplet diameter changes from 1550 to 1200 nm and finally to 600 nm (Figure 4g−i). For the 1550 nm droplet, the central 1 μm square region adopts a polydomain structure similar to that observed for thin films. In contrast, the 600 nm droplet has a small polydomain region of nanodots at the center, with the majority of the droplet forming a defective topographic structure. Toward the droplet edge, defects become more prevalent and the natural periodicity (L_0) is lost with the emergence of parallel PMMA cylinders at the periphery. In a planar continuous film, the hexagonal pattern is free to form well-ordered domains. In a droplet configuration, to account for its radial nature and convex shape, a higher number of defects are expected due to compression of the polymer chains. To gain a better understanding of the reorientation of the PMMA cylinders at the edge, it is appropriate to first investigate the formation of sub-400 nm microdroplets as these systems can provide an insight into the reorientation.

Nanoring Formation. By extending the mesa widths to larger dimensions, and as a consequence of the unique geometry of the top-down (via-holes) and bottom-up (microdroplets) structures, oblique nanorings, whereby the PMMA cylinders produced concentric rings parallel to the substrate, were formed. Figure 5a−d displays tilt SEM images for two different pitch and via-hole spacings of the SSQ prepatterns and the resultant microdroplet structures. Beyond via-spacer dimensions of ~1.4 μm, as highlighted in Figure 5b,d, it is possible to create self-aligned, self-supporting nanorings with long axis dimensions ranging from 250 to 350 nm with preferred cylinder orientations. At this stage, the microdroplet also begins to adopt a rounded square shape, which is attributed to the method of film rupture during dewetting. Briefly, annealing the block copolymer films for 24 h provides adequate time for the mass flow of the BCP to form the arrays of microdroplets. Figure 5e highlights a structure formed during 6 h of annealing where insufficient time has elapsed for the array of microdroplets to form. However, the image does provide insight into the dewetting mechanism and how nanorings form as a result. During the initial stages of thermal annealing, polymer around the via-hole flows equally into the via-hole structures as a result of capillary forces.[58] As two neighboring via-holes simultaneously pull polymer from the shared mesa (while polymer also moves to the interstitial mesa sites), a thin ridge forms between the two neighboring via-holes until mass transport is complete. If the distance from via-hole to via-hole for polymer flow is too great, then polymer will remain behind to form small droplets and ultimately produce nanorings. The registration of the nanorings to neighboring microdroplets and via-holes has a placement error of ~10%, as highlighted in Figure 5f,g. Figure 5g is a grid map of Figure 5f, which highlights the placement error and nanoring misalignment direction angle (φ). The droplet's long axis runs orthogonal to the hole-to-hole direction, with some droplets deviating from this direction (φ) by no more than 15°. In most cases, the droplet registers with both the via-hole and microdroplet. Regrettably, the process was not homogeneous across the entire array of holes as nanorings did not develop in all available sites (Figure 5b). The process of forming microdroplets, which subsequently form nanoring structures at all available sites, requires precise delivery of polymer to all sites and strict control over variables such as temperature and the physical prepatterns, but most importantly, it necessitates that the adjacent microdroplets must adopt precise positions, sizes, and shapes. Further examination of the nanorings in Figure 5h,i reveals that the PMMA cylinders form aperiodic ring structures arranged parallel to the substrate within the PS matrix. The natural periodicity (L_0) for parallel cylinders of ~40 nm cannot be sustained as the film thickness varies across the nanoring. Extrapolating the droplet thickness for a 300 nm droplet from FIB data (Supporting Information section S2) suggests most of the droplet thickness is submonolayer (*i.e.*, below L_0). As previously determined, cylinders are oriented parallel to the substrate with the PS component wetting the SSQ interface. The outer PS segment has the highest domain spacing of 53 nm as film thickness changes are most pronounced at the edge. The next domain spacing of 34 nm is

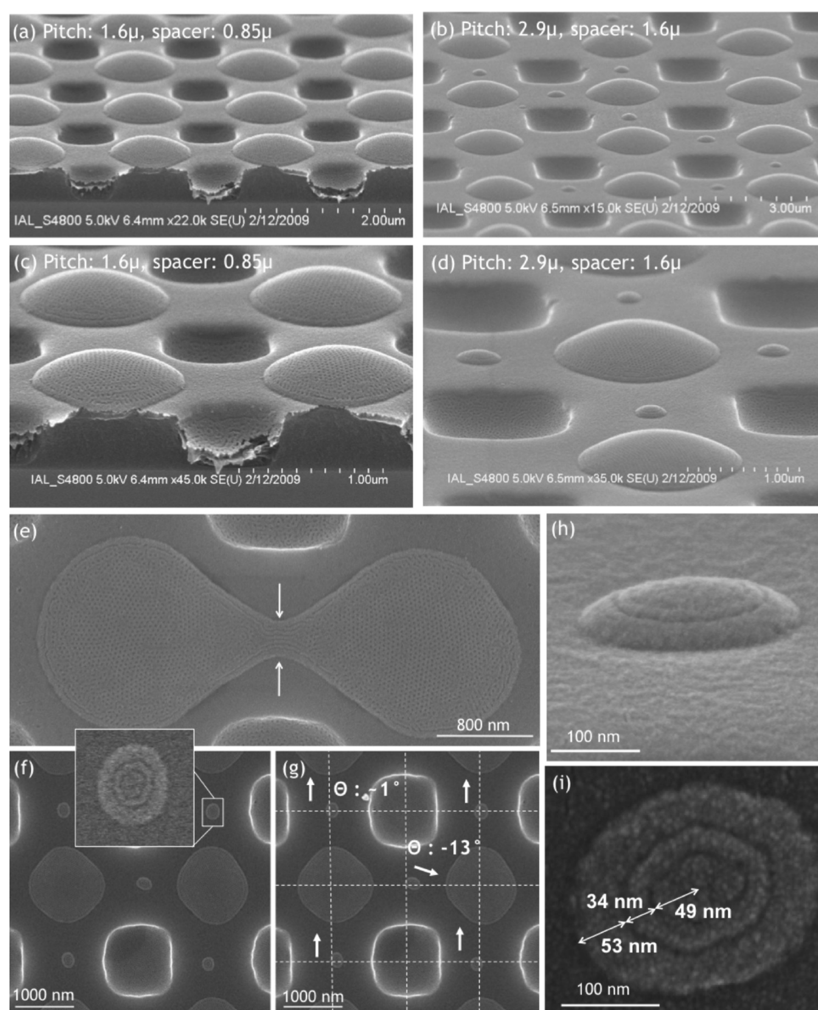

Figure 5. Nanoring formation: (a−d) 70° tilt SEM images of nanoring formation by controlling the spacing between microdroplets. Images (c) and (d) are higher magnifications of (a) and (b). (e) Insight into dewetting mechanism and nanoring formation by observing the formation of thin polymer ridges after annealing for 6 h highlighted by two arrows. (f) Top-down SEM image of five nanorings and (g) superimposed boundaries to emphasize *XY* positional and directionality error of the five nanorings. SEM images (h) and (i) of aperiodic, self-aligned, and self-supporting nanorings with concentric parallel PMMA cylinders.

considerably smaller than the natural periodicity, while the internal PS core has a radius of 49 nm. The ability of block copolymers to bend and form such nanoring structures has been observed for nanorings formed by both graphoepitaxy[33] and chemiepitaxy[30,34] techniques, but indirectly templated, isolated, and registered freestanding nanorings have yet to be reported.

Confining block copolymers in cylindrical pores of anodic alumina membranes,[59] *via* micrometer-sized trenches[33] or through dewetting processes,[60] has been shown to affect the morphology of the system. For the PS-*b*-PMMA on SSQ surfaces, the ability of the droplets to undergo a reorientation at the periphery was driven by the in-plane radial curvature of the droplet and not the droplet thickness; although droplet thickness is a necessity for the reorientation process to occur, a high in-plane radius of curvature is required to induce the reorientation. Figure 6 displays SEM top-down and 70° tilt images of the microdroplets with size ranging from 200 to 2000 nm. At high droplet diameters (*ca.* 2000 nm), the droplet adopts a rounded square shape. At these corners, in-plane radial curvature is significant and parallel cylinders are observed at these locations (white arrows throughout Figure 6). As the droplet shrinks in size, the in-plane radial curvature becomes greater and parallel cylinders are frequently observed and in some cases extend the full circumference of the droplets (Figure 6g). At droplet dimensions of 250 nm (Figure 6h), only PMMA cylinders with parallel orientation are observed. Previously, Heier *et al.* observed this phenomenon within sub-1 μm droplets of PS-*b*-PVP. The authors suggested that the reorientation was a result of the increase of free energy per unit volume, which originated from the line tension at the periphery of the droplet. Previous reports have shown that subtle changes in film thickness can result in abrupt changes in cylinder orientation.[45,56] Such behavior has previously been shown for varying film thicknesses with PS-*b*-PMMA films,[45] where hybrid and half cylinder structures formed

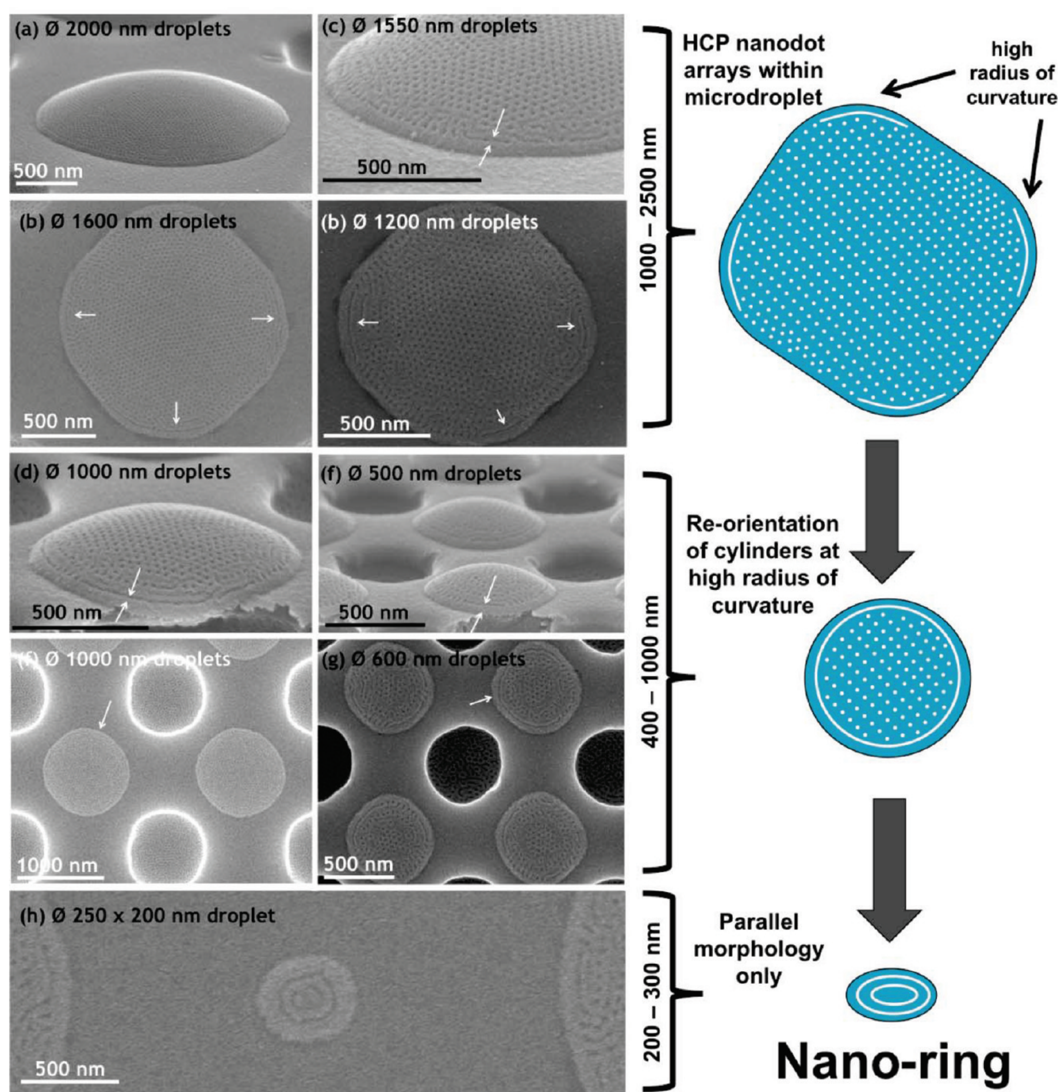

Figure 6. Cylinder reorientation. SEM top-down and 70° tilt images highlighting the cylinder reorientation at droplet edge where a high radius of curvature is present. As droplet size decreases, the radius of curvature becomes pronounced, leading to nanoring formation. White arrows indicate regions where parallel cylinders are observed at the droplet edge.

when the thickness was sub-L_0. Interestingly, Fasolka and co-workers[56] studied lamellar PS-*b*-PLMA (polystyrene-*block*-poly(lauryl methacrylate)) droplets, using TEM staining and AFM techniques, and observed a range of hybrid structures below L_0. For all droplet sizes, the droplet thickness at the edge was extremely thin and the domain spacings were expanded. Again, and similar to the periodicities of the microdroplets, the periodicity from the edge to the first row of dots/cylinders and, consequently, to the second row of dots is stretched, with values of 50 to 55 nm recorded. These larger values may be caused by a morphological change or packing frustration of the chains as the thickness is well below the natural periodicity.

CONCLUSION

Silsesquioxane prepatterns made possible by NIL, which combine chemical and physical properties, are extremely useful substrates for controlling dewetting processes and, ultimately, the formation of hierarchal structures. Tunable microdroplet arrays, with droplet sizes ranging from 250 to 3000 nm, can be fabricated with relative ease by preprogramming the SSQ via-hole dimensions. Although the microdroplets are microphase separated, the ordering of the hexagonal closed-packed arrangement on the surface is limited by the convex nature of the droplet. The out-of-plane radius of curvature of the droplet itself may also cause a cylinder to spherical domain transition, but the observation of such a transition ultimately requires more advanced microscopy investigations (TEM and staining). Directional, self-supporting (template-free), and self-aligned nanorings are produced when microdroplets are placed beyond a critical distance (1.4 μm). The nanoring droplets adopt an aperiodic polydomain structure as the radius of curvature is pronounced at these dimensions. The cylinder reorientation process was driven by the high in-plane radius of curvature and was not governed by thickness effects. Future

studies will involve precision template fabrication by NIL to create square trench and via-hole profiles, while work will also focus on delivering controlled amounts of polymer to the substrate to ensure nanoring formation is continuous and each interstitial site is occupied. By utilizing both the trench and the mesa surface regions, our approach may hold advantages over other patterning techniques, namely, graphoepitaxy, as magnetic nanorings could be fabricated on both the mesa and within the template thereby increasing the areal density.

EXPERIMENTAL SECTION

SSQ Substrate Fabrication and RUV-NIL. The synthesis of the UV-curable silsesquioxane (SSQ) is reported elsewhere.[61] Polyhedral silsesquioxane (SSQ) cages bearing eight dimethylsilyloxy groups were functionalized with polymerizable groups by a hydrosilylation reaction carried out on the Si−H functional group. A polyhedral silsesquioxane with a six-alkyl chain length with a viscosity of 0.9 Pa·s in toluene was used for all RUV-NIL experiments. Resist patterns were created on a quartz substrate by thermal nanoimprint lithography. A PMMA layer was spin-coated at 3000 rpm on a quartz substrate and imprinted at 180 °C for 5 min under a pressure of 50 bar. The stamp and substrate where separated at 100 °C, and the residual PMMA layer removed by an oxygen-based RIE. Eighty nanometers of chromium was evaporated onto the opened resist patterns by electron beam evaporation (Temescal 2000F), and the finalized chromium patterns were realized by lift-off. A sacrificial lift-off resist (LOR, MicroChem Corp) was deposited at 3000 rpm on top of the metal arrays to enable effective release after imprinting. The mask was completed by spin-coating the SSQ onto the sacrificial polymer at 1500 rpm. Next, the mask layer was imprinted onto a brush-coated 30 × 30 mm silicon substrate. The brush was a 1 wt % solution of random copolymer of polystyrene-*random*-poly(methyl methylacrylate) (PS-*r*-PMMA) with a polystyrene content of 58% and was purchased from Polymer Source Inc. of Quebec, Canada. PS-*r*-PMMA was grafted to the silicon substrate by spin-coating at 4000 rpm, annealing the thin film at 180 °C (48 h) under vacuum, and removing the excess polymer by repeated immersion in toluene three times under sonication. An RUV-NIL technique was employed to fabricate the SSQ templates using a 2.5 in. Obducat nanoimprint system under a pressure of 6 bar for 60 s followed by a 5 s UV polymerization ($\lambda = 250-400$ nm) step to cross-link the siloxane structure. Development of the SSQ was performed in 0.1 M tetramethylammoniumhydroxide (TMAOH) for 2 min and rinsed under flowing deionized water for an additional 2 min. All spin-coating was performed on a Specialty Coating Systems G3P-8 spin-coater.

Deposition and Thin Film Formation. Polystyrene-*block*-poly-(methyl methylacrylate) (PS-*b*-PMMA) with a polystyrene content of 0.72 and a M_n value of 67.0 kg/mol was purchased from Polymer Source Inc. of Quebec (Canada) and used as received. One weight percent PS-*b*-PMMA in toluene solutions was spin-coated using a Specialty Coating Systems G3P-8 spin-coater at 3000 rpm onto the patterned SSQ films unless otherwise noted. Simultaneous microphase separation and dewetting was achieved by placing the films in a vacuum oven for 24 h at 180 °C. For planar films, where hexagonal cylinders of PMMA were oriented perpendicular to the substrate, a random copolymer of polystyrene-*random*-poly(methyl methylacrylate) (PS-*r*-PMMA) was employed as outlined in the previous section.

Thin Film and Microdroplet Characterization. SEM images were obtained using Hitachi S4800 and FEI Strata DualBeam 235 microscopes operating at accelerating voltages of 2−5 kV. To improve SEM contrast, partial removal of the PMMA was performed by dry etching with an Oxford Plasmatech 100 using an oxygen/trifluoromethane (O_2/CHF_3) mixture for 20 s at a base pressure of 0.1 mTorr at 10 °C. Loss of PS was negligible in comparison to the PMMA, and the etch rate for PMMA was 25 nm per min. In order to minimize charging effects, samples were coated with a thin layer of Au/Pd deposited by sputtering methods. FIB cross-sectional samples were prepared using an FEI Strata DualBeam 235 system. Contact angle measurements were determined on a DataPhysics OCA30 system operating in static mode according to the sessile drop method. Optical images of the polymer microdroplet arrays were recorded on a Zeiss Axioskop 40 Pol optical microscope.

Acknowledgment. The authors acknowledge the following sources of funding which supported this work: SFI Grant 03-IN3-I375, SFI CRANN CSET grant, and NaPANIL FP7-CP-IP 214249. The authors are grateful to Intel Ireland for access to microscopy facilities and continuous support. Access to fabrication facilities (plasma processing) was partly funded by the SFI National Access Program at the Tyndall National Institute (Project Number 132).

Supporting Information Available: Initial graphoepitaxy investigations, SEM/FIB cross sections of microdroplets, and statistical analysis of pitch periodicities of various droplet sizes. This material is available free of charge *via* the Internet at http://pubs.acs.org.

REFERENCES AND NOTES

1. Hamley, I. W. Nanostructure Fabrication Using Block Copolymers. *Nanotechnology* **2003,** *14*, R39.
2. Han, E.; Stuen, K. O.; Leolukman, M.; Liu, C. C.; Nealey, P. F.; Gopalan, P. Perpendicular Orientation of Domains in Cylinder-Forming Block Copolymer Thick Films by Controlled Interfacial Interactions. *Macromolecules* **2009,** *42*, 4896.
3. Thurn-Albrecht, T.; Schotter, J.; Kastle, C. A.; Emley, N.; Shibauchi, T.; Krusin-Elbaum, L.; Guarini, K.; Black, C. T.; Tuominen, M. T.; Russell, T. P. Ultrahigh-Density Nanowire Arrays Grown in Self-Assembled Diblock Copolymer Templates. *Science* **2000,** *290*, 2126.
4. Black, C. T.; Ruiz, R.; Breyta, G.; Cheng, J. Y.; Colburn, M. E.; Guarini, K. W.; Kim, H. C.; Zhang, Y. Polymer Self Assembly in Semiconductor Microelectronics. *IBM J. Res. Dev.* **2007,** *51*, 605.
5. Kim, S. O.; Solak, H. H.; Stoykovich, M. P.; Ferrier, N. J.; de Pablo, J. J.; Nealey, P. F. Epitaxial Self-Assembly of Block Copolymers on Lithographically Defined Nanopatterned Substrates. *Nature* **2003,** *424*, 411.
6. Cheng, J. Y.; Sanders, D. P.; Truong, H. D.; Harrer, S.; Friz, A.; Holmes, S.; Colburn, M.; Hinsberg, W. D. Simple and Versatile Methods To Integrate Directed Self-Assembly with Optical Lithography Using a Polarity-Switched Photoresist. *ACS Nano* **2010,** *4*, 4815.
7. Jeong, S. J.; Moon, H. S.; Kim, B. H.; Kim, J. Y.; Yu, J.; Lee, S.; Lee, M. G.; Choi, H.; Kim, S. O. Ultralarge-Area Block Copolymer Lithography Enabled by Disposable Photoresist Prepatterning. *ACS Nano* **2010,** *4*, 5181.
8. Li, H. W.; Huck, W. T. S. Ordered Block-Copolymer Assembly Using Nanoimprint Lithography. *Nano Lett.* **2004,** *4*, 1633.
9. Reiter, G. Dewetting of Thin Polymer-Films. *Phys. Rev. Lett.* **1992,** *68*, 75.
10. Reiter, G. Unstable Thin Polymer Films: Rupture and Dewetting Processes. *Langmuir* **1993,** *9*, 1344.
11. Xie, R.; Karim, A.; Douglas, J. F.; Han, C. C.; Weiss, R. A. Spinodal Dewetting of Thin Polymer Films. *Phys. Rev. Lett.* **1998,** *81*, 1251.
12. Seemann, R.; Herminghaus, S.; Jacobs, K. Gaining Control of Pattern Formation of Dewetting Liquid Films. *J. Phys.: Condens. Matter* **2001,** *13*, 4925.
13. Limary, R.; Green, P. F. Dewetting Instabilities in Thin Block Copolymer Films: Nucleation and Growth. *Langmuir* **1999,** *15*, 5617.

14. Lu, G.; Li, W.; Yao, J. M.; Zhang, G.; Yang, B.; Shen, J. C. Fabricating Ordered Two-Dimensional Arrays of Polymer Rings with Submicrometer-Sized Features on Patterned Self-Assembled Monolayers by Dewetting. *Adv. Mater.* **2002,** *14*, 1049.
15. Zhang, Z. X.; Wang, Z.; Xing, R. B.; Han, Y. C. How To Form Regular Polymer Microstructures by Surface-Pattern-Directed Dewetting. *Surf. Sci.* **2003,** *539*, 129.
16. Pai, I. T.; Chiou, D. W.; Hon, M. H.; Leu, I. C. Hierarchical Structure Formation Induced by Dewetting in an Imprinting Process. *J. Vac. Sci. Technol., B* **2009,** *27*, 2858.
17. Zhu, J. T.; Zhao, J. C.; Liao, Y. G.; Jiang, W. Multiscale Dewetting of Triblock Copolymer Thin Film Induced by Solvent Vapor. *J. Polym. Sci., Part B* **2005,** *43*, 2874.
18. Lee, S. H.; Kang, H. M.; Kim, Y. S.; Char, K. Hierarchical Surface Topography in Block Copolymer Thin Films Induced by Residual Solvent. *Macromolecules* **2003,** *36*, 4907.
19. Hamley, I. W.; Hiscutt, E. L.; Yang, Y. W.; Booth, C. Dewetting of Thin Block Copolymer Films. *J. Colloid Interface Sci.* **1999,** *209*, 255.
20. Hahm, J.; Sibener, S. J. Cylinder Alignment in Annular Structures of Microphase-Separated Polystyrene-*b*-Poly(methyl methacrylate). *Langmuir* **2000,** *16*, 4766.
21. Croll, A. B.; Massa, M. V.; Matsen, M. W.; Dalnoki-Veress, K. Droplet Shape of an Anisotropic Liquid. *Phys. Rev. Lett.* **2006,** *97*, 204502.
22. Croll, A. B.; Dalnoki-Veress, K. Spreading of Diblock Copolymer Droplets: A Probe of Polymer Micro-Rheology. *Eur. Phys. J. E* **2009,** *29*, 239.
23. Hong, S. W.; Wang, J.; Lin, Z. Evolution of Ordered Block Copolymer Serpentines into a Macroscopic, Hierarchically Ordered Web. *Angew. Chem., Int. Ed.* **2009,** *48*, 8356.
24. Ramanathan, M.; Darling, S. B. Thickness Dependent Hierarchical Meso/Nanoscale Morphologies of a Metal-Containing Block Copolymer Thin Film Induced by Hybrid Annealing and Their Pattern Transfer Abilities. *Soft Matter* **2009,** *5*, 4665.
25. Xu, L.; Yu, X. F.; Shi, T. F.; An, L. J. Investigation of the Dewetting Inhibition Mechanism of Thin Polymer Films. *Soft Matter* **2009,** *5*, 2109.
26. Kim, T. H.; Hwang, J.; Hwang, W. S.; Huh, J.; Kim, H. C.; Kim, S. H.; Hong, J. M.; Thomas, E. L.; Park, C. Hierarchical Ordering of Block Copolymer Nanostructures by Solvent Annealing Combined with Controlled Dewetting. *Adv. Mater.* **2008,** *20*, 522.
27. Kim, B. H.; Shin, D. O.; Jeong, S. J.; Koo, C. M.; Jeon, S. C.; Hwang, W. J.; Lee, S.; Lee, M. G.; Kim, S. O. Hierarchical Self-Assembly of Block Copolymers for Lithography-Free Nanopatterning. *Adv. Mater.* **2008,** *20*, 2303.
28. Kim, B. H.; Lee, H. M.; Lee, J. H.; Son, S. W.; Jeong, S. J.; Lee, S.; Il Lee, D.; Kwak, S. U.; Jeong, H.; Shin, H.; *et al.* Spontaneous Lamellar Alignment in Thickness-Modulated Block Copolymer Films. *Adv. Funct. Mater.* **2009,** *19*, 2584.
29. Yamaguchi, T.; Yamaguchi, H. Two-Dimensional Patterning of Flexible Designs with High Half-Pitch Resolution by Using Block Copolymer Lithography. *Adv. Mater.* **2008,** *20*, 1684.
30. Cheng, J. Y.; Rettner, C. T.; Sanders, D. P.; Kim, H. C.; Hinsberg, W. D. Dense Self-Assembly on Sparse Chemical Patterns: Rectifying and Multiplying Lithographic Patterns Using Block Copolymers. *Adv. Mater.* **2008,** *20*, 3155.
31. Grigorescu, A. E.; Hagen, C. W. Resists for Sub-20-nm Electron Beam Lithography with a Focus on HSQ: State of the Art. *Nanotechnology* **2009,** *20*, 292001.
32. Sim, J. H.; Lee, S. I.; Lee, H. J.; Kasica, R.; Kim, H. M.; Soles, C. L.; Kim, K. B.; Yoon, D. Y. Novel Organosilicate Polymer Resists for High Resolution E-Beam Lithography. *Chem. Mater.* **2010,** *22*, 3021.
33. Chuang, V. P.; Ross, C. A.; Bilalis, P.; Hadjichristidis, N. Nanoscale Rings Fabricated Using Self-Assembled Triblock Terpolymer Templates. *ACS Nano* **2008,** *2*, 2007.
34. Wilmes, G. M.; Durkee, D. A.; Balsara, N. P.; Liddle, J. A. Bending Soft Block Copolymer Nanostructures by Lithographically Directed Assembly. *Macromolecules* **2006,** *39*, 2435.
35. Subramani, A.; Geerpuram, D.; Domanowski, A.; Baskaran, V.; Medushko, V. Vortex State in Magnetic Rings. *Physica C* **2004,** *404*, 241.
36. Park, S.; Wang, J.-Y.; Kim, B.; Russell, T. P. From Nanorings to Nanodots by Patterning with Block Copolymers. *Nano Lett.* **2008,** *8*, 1667.
37. O'Driscoll, S. M.; O'Mahony, C. T.; Farrell, R. A.; Fitzgerald, T. G.; Holmes, J. D.; Morris, M. A. Toroid Formation in Polystyrene-*block*-Poly(4-vinyl pyridine) Diblock Copolymers: Combined Substrate and Solvent Control. *Chem. Phys. Lett.* **2009,** *476*, 65.
38. Kehagias, N.; Reboud, V.; Chansin, G.; Zelsmann, M.; Jeppesen, C.; Schuster, C.; Kubenz, M.; Reuther, F.; Gruetzner, G.; Torres, C. M. S. Reverse-Contact UV Nanoimprint Lithography for Multilayered Structure Fabrication. *Nanotechnology* **2007,** *18*, 175303.
39. Coulon, G.; Daillant, J.; Collin, B.; Benattar, J. J.; Gallot, Y. Time Evolution of the Free-Surface of Ultrathin Copolymer Films. *Macromolecules* **1993,** *26*, 1582.
40. Mansky, P.; Russell, T. P.; Hawker, C. J.; Mays, J.; Cook, D. C.; Satija, S. K. Interfacial Segregation in Disordered Block Copolymers: Effect of Tunable Surface Potentials. *Phys. Rev. Lett.* **1997,** *79*, 237.
41. Wu, S. *Polymer Interface and Adhesion*; Marcel Dekker Inc: New York, 1982.
42. Morkved, T. L.; Lopes, W. A.; Hahm, J.; Sibener, S. J.; Jaeger, H. M. Silicon Nitride Membrane Substrates for the Investigation of Local Structure in Polymer Thin Films. *Polymer* **1998,** *39*, 3871.
43. Black, C. T. Self-Aligned Self Assembly of Multi-Nanowire Silicon Field Effect Transistors. *Appl. Phys. Lett.* **2005,** *87*, 163116.
44. Jeong, S. J.; Kim, J. E.; Moon, H. S.; Kim, B. H.; Kim, S. M.; Kim, J. B.; Kim, S. O. Soft Graphoepitaxy of Block Copolymer Assembly with Disposable Photoresist Confinement. *Nano Lett.* **2009,** *9*, 2300.
45. Kim, H. C.; Russell, T. P. Ordering in Thin Films of Asymmetric Diblock Copolymers. *J. Polym. Sci., Part B* **2001,** *39*, 663.
46. Mansky, P.; Liu, Y.; Huang, E.; Russell, T. P.; Hawker, C. J. Controlling Polymer−Surface Interactions with Random Copolymer Brushes. *Science* **1997,** *275*, 1458.
47. Huang, E.; Russell, T. P.; Harrison, C.; Chaikin, P. M.; Register, R. A.; Hawker, C. J.; Mays, J. Using Surface Active Random Copolymers to Control the Domain Orientation in Diblock Copolymer Thin Films. *Macromolecules* **1998,** *31*, 7641.
48. Ryu, D. Y.; Ham, S.; Kim, E.; Jeong, U.; Hawker, C. J.; Russell, T. P. Cylindrical Microdomain Orientation of PS-*b*-PMMA on the Balanced Interfacial Interactions: Composition Effect of Block Copolymers. *Macromolecules* **2009,** *42*, 4902.
49. Aissou, K.; Kogelschatz, M.; Baron, T. Self-Assembling Study of a Cylinder-Forming Block Copolymer *via* a Nucleation-Growth Mechanism. *Nanotechnology* **2009,** *20*, 095602.
50. Aissou, K.; Kogelschatz, M.; Baron, T.; Gentile, P. Self-Assembled Block Polymer Templates as High Resolution Lithographic Masks. *Surf. Sci.* **2007,** *601*, 2611.
51. Ruiz, R.; Kang, H. M.; Detcheverry, F. A.; Dobisz, E.; Kercher, D. S.; Albrecht, T. R.; de Pablo, J. J.; Nealey, P. F. Density Multiplication and Improved Lithography by Directed Block Copolymer Assembly. *Science* **2008,** *321*, 936.
52. Kobayashi, H. Surface-Tension of Poly(fluoroalkylsilsesquioxane). *Macromol. Chem. Phys.* **1993,** *194*, 2569.
53. Welander, A. M.; Nealey, P. F.; Cao, H.; Bristol, R. Impact of Trench Width Roughness on the Graphoepitaxial Assembly of Block Copolymers. *J. Vac. Sci. Technol., B* **2008,** *26*, 2484.
54. Bita, I.; Yang, J. K. W.; Jung, Y. S.; Ross, C. A.; Thomas, E. L.; Berggren, K. K. Graphoepitaxy of Self-Assembled Block Copolymers on Two-Dimensional Periodic Patterned Templates. *Science* **2008,** *321*, 939.
55. Suh, H. S.; Kang, H. M.; Liu, C. C.; Nealey, P. F.; Char, K. Orientation of Block Copolymer Resists on Interlayer Dielectrics with Tunable Surface Energy. *Macromolecules* **2010,** *43*, 461.

56. Fasolka, M. J.; Banerjee, P.; Mayes, A. M.; Pickett, G.; Balazs, A. C. Morphology of Ultrathin Supported Diblock Copolymer Films: Theory and Experiment. *Macromolecules* **2000,** *33*, 5702.
57. Liu, G. L.; Kang, H. M.; Craig, G. S. W.; Detcheverry, F.; de Pablo, J. J.; Nealey, P. F.; Tada, Y.; Yoshida, H. Cross-Sectional Imaging of Block Copolymer Thin Films on Chemically Patterned Surfaces. *J. Photopolym. Sci. Technol.* **2010,** *23*, 149.
58. Fitzgerald, T. G.; Farrell, R. A.; Petkov, N.; Bolger, C. T.; Shaw, M. T.; Charpin, J. P. F.; Gleeson, J. P.; Holmes, J. D.; Morris, M. A. Study on the Combined Effects of Solvent Evaporation and Polymer Flow upon Block Copolymer Self-Assembly and Alignment on Topographic Patterns. *Langmuir* **2009,** *25*, 13551.
59. Shin, K.; Xiang, H. Q.; Moon, S. I.; Kim, T.; McCarthy, T. J.; Russell, T. P. Curving and Frustrating Flatland. *Science* **2004,** *306*, 76.
60. Thomas, E. L.; Reffner, J. R.; Bellare, J. A Menagerie of Interface Structures in Copolymer Systems. *J. Phys.* **1990,** *51*, C7363.
61. Crivello, J. V.; Malik, R. Synthesis and Photoinitiated Cationic Polymerization of Monomers with the Silsesquioxane Core. *J. Polym. Sci., Part A* **1997,** *35*, 407.